A Generalized Multicarrier Communication System – Part II: The T-OFDM System

Imran Ali
self@ImranAliPhD.com
Independent Researcher, Melbourne, Australia

Abstract
Precoding of the orthogonal frequency division multiplexing (OFDM) with Walsh Hadamard transform (WHT) is known in the literature. Instead of performing WHT precoding and inverse discrete Fourier transform separately, a product of two matrix can yield a new matrix that can be applied with lower complexity. This resultant transform, *T*-transform, results in T-OFDM. This paper extends the limited existing work on T-OFDM significantly by presenting detailed account of its computational complexity, a lower complexity receiver design, an expression for PAPR and its cumulative distribution function (cdf), sensitivity of T-OFDM to timing synchronization errors, and novel analytical expressions signal to noise ratio (SNR) for multiple equalization techniques. Simulation results are presented to show significant improvements in PAPR performance, as well improvement in bit error rate (BER) in Rayleigh fading channel. This paper is Part II of a three-paper series on alternative transforms and many of the concepts and result refer to and stem from results in generalized multicarrier communication (GMC) system presented in Part I of this series.
Keywords:
Walsh Hadamard, OFDM, PAPR, T-OFDM

1. Introduction

The conventional orthogonal frequency division multiplexing (OFDM), a multicarrier communication (MC) system is the choice of modulation in many communication standards [1], [2]. The conventional OFDM uses a discrete Fourier transform (DFT) pair at transmitter and receiver, coupled with cyclic prefix (CP) insertion, such that transfer matrix of multipath fading channel becomes circulant, whose eigenvectors are inverse and forward DFT matrices, thereby diagonalizing it and resulting in a single-tap equalization. The OFDM also offers benefits from better spectral efficiency due to partially overlapping and still orthogonal subcarriers [3] and lower sensitivity to timing synchronization errors [4]. However, it suffers significant challenges in its inability to harvest channel diversity [5], unlike its predecessor single carrier systems, as well as high peak to average power ratio [6] and sensitivity to carrier frequency offset (CFO) [7].

To address these drawbacks, myriad approaches have been employed in the literature, including some form of precoding [8], channel coding [9], pilot signal [10], amongst others. Use of alternative transform is one these techniques, although a less popular one. For example, real valued trigonometric transform was used in OFDM in [11], which had an advantage in situation when channel delay spread is longer than cyclic prefix but disadvantage of being real value, so unable to use complex two-dimensional alphabets for modulation, thereby compromising on overall spectral efficiency. A similar real value discrete Hartley transform (DHT) based OFDM was proposed in [12] and [13].

Precoding conventional OFDM with WHT matrix has appeared in the literature, in for example, [14] and [15], which demonstrate improvement in PAPR and [16] shows improvement in BER performance using simulation results and [15] and [16] presents and iterative minimum mean square error (MMSE) is presented in [17]. The idea of combining WHT and DFT transforms into *T*-transform was first published in [14] showing lower computational complexity. However, since *T*-transform cannot diagonalize the channel matrix (see [18], *Theorem 3*), a Hadamard domain equalization using dyadic convolution was proposed in [19] with a computational complexity of $O(N^2)$, where N is the number of subcarriers. A lower complexity receiver was designed in [15], where the transmitter and receiver side transform were splits, with equalization in between, thereby increasing transform complexity but reducing equalization complexity significantly so that overall complexity is reduced. This paper extends the work in T-OFDM significantly by making several contributions described below.

A. Contributions of this Paper

Following are the contributions of this paper.

a) Expression for diversity order attained by T-OFDM is derived, showing its ability to harvest full channel diversity.
b) An expression is derived for the coding gain attained by T-OFDM is also derived.
c) An expression for per subcarrier SNR for ZF equalizer is derived for T-OFDM

Manuscript received September 5, 2024
Manuscript revised September 20, 2024
https://doi.org/10.22937/IJCSNS.2024.24.9.3

d) An expression for per subcarrier signal to noise plus interference (SINR) is derived for each subchannel with MMSE receiver.

e) It demonstrated both analytically and simulation results that, unlike conventional OFDM, the T-OFDM suffers from greater penalty due to the timing synchronization errors.

The remainder of this paper is organized as follows. In Section 2, T-OFDM signal model is presented, along with various receiver designs, their equivalency and improved BER performance, and the T-transform structure and complexity are presented. The analysis of PAPR is carried out in Section 3, where Section 4 focuses on error performance, including detail analysis for ZF and MMSE receivers. Section 5 focuses on timing synchronization errors, while Section 6 concludes this paper.

2. The T-OFDM System

The block diagram of T-OFDM system is given in Figure 1. The T-OFDM system is based upon the T-transform pair, such that it is a special case of generalized multicarrier communication (GMC) system introduced in Part I [18] of this three-paper series, with $\boldsymbol{Q}_T = \boldsymbol{T}^{\mathcal{H}}$, where

$$\begin{aligned} \boldsymbol{T}^{\mathcal{H}} &\triangleq \boldsymbol{F}^{\mathcal{H}}\boldsymbol{W}^{\mathcal{H}} = \boldsymbol{F}^{\mathcal{H}}\boldsymbol{W} \qquad (\because \boldsymbol{W}^{\mathcal{H}} = \boldsymbol{W}), \\ \boldsymbol{T} &\triangleq \boldsymbol{W}\boldsymbol{F} = \boldsymbol{W}^{\mathcal{H}}\boldsymbol{F}, \end{aligned} \tag{1}$$

where $\boldsymbol{W}$ is the Walsh-Hadamard transform (WHT) matrix, such that its $(u,v)^{\text{th}}$ entry is $[\boldsymbol{W}]_{u,v} = \frac{1}{\sqrt{N}}\prod_{i=0}^{c-1}(-1)^{u_i v_i}$, where u_i and v_i are the i^{th} bits of the binary representation of u and v respectively and $c = \log_2 N$.

The transmitter of the system utilizes the inverse T-transform and cyclic prefix (CP) insertion, so that the i^{th} transmitted symbol is given as $\boldsymbol{x}_{\text{cp}} = \boldsymbol{\Xi}_I \boldsymbol{T}^{\mathcal{H}}\boldsymbol{X}$, where $\boldsymbol{\Xi}_I$ is the CP insertion matrix. The channel matrix becomes circulant because of the use of CP so that the received vector after the CP removal is given as,

$$\boldsymbol{y} = \boldsymbol{H}_c \boldsymbol{T}^{\mathcal{H}}\boldsymbol{X} + \boldsymbol{\eta}. \tag{2}$$

Three different receiver configurations for T-OFDM are shown in Figure 1. The receiver configuration in $1(b)$, hereafter referred to as dyadic convolution receiver, was the proposed receiver of T-OFDM in the original work of [16]. In the dyadic convolution receiver, the T -transform is implemented first at the receiver, to get,

$$\begin{aligned} \boldsymbol{Y} &= \boldsymbol{T}\boldsymbol{H}_c\boldsymbol{T}^{\mathcal{H}}\boldsymbol{X} + \boldsymbol{T}\boldsymbol{\eta} \\ &= \boldsymbol{W}\boldsymbol{F}\boldsymbol{H}_c\boldsymbol{F}^{\mathcal{H}}\boldsymbol{W}\boldsymbol{X} + \boldsymbol{W}\boldsymbol{w} \quad (\text{recall } \boldsymbol{w} \triangleq \boldsymbol{F}\boldsymbol{\eta}) \\ &= \boldsymbol{W}\boldsymbol{D}\boldsymbol{W}\boldsymbol{X} + \boldsymbol{W}\boldsymbol{w} \end{aligned} \tag{3}$$

where $\boldsymbol{D} = \boldsymbol{F}\boldsymbol{H}_c\boldsymbol{F}^{\mathcal{H}}$ has been used. The matrix $\boldsymbol{W}\boldsymbol{D}$ is not diagonal, so single-tap equalization is not possible.

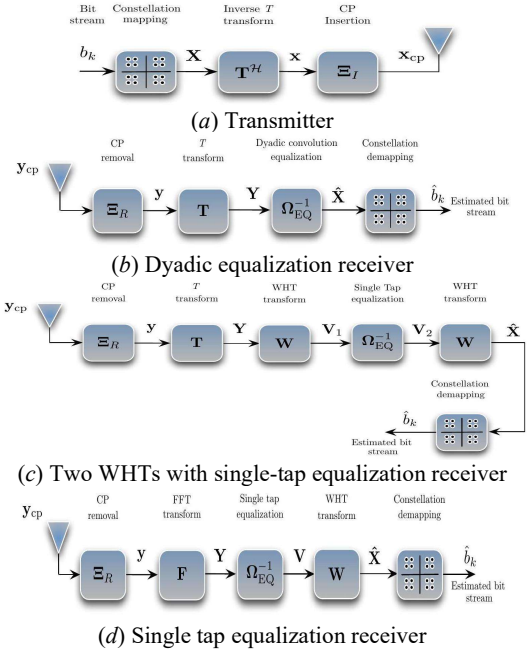

(*a*) Transmitter

(*b*) Dyadic equalization receiver

(*c*) Two WHTs with single-tap equalization receiver

(*d*) Single tap equalization receiver

Figure 1: Block diagrams of T-OFDM system with different receiver configurations

It has been shown in [20] that, if $\boldsymbol{a}$ and $\boldsymbol{b}$ are two vectors such that $\boldsymbol{A} \triangleq \boldsymbol{W}\boldsymbol{a}$ and $\boldsymbol{B} \triangleq \boldsymbol{W}\boldsymbol{b}$, then

$$[\boldsymbol{A}]_k[\boldsymbol{B}]_k = \sum_{n=0}^{N-1} [\boldsymbol{a}]_{k\oplus n}[\boldsymbol{b}]_n, \tag{4}$$

where the binary operation $\{\cdot\} \oplus \{\cdot\}$ involves the processes of converting both integer argument to binary numbers, performing exclusive-OR operation between the two binary streams and converting the result back into decimal number. The right-hand side of Equation (4) is called logical or dyadic convolution, such that the Equation (4) represents the logical convolution theorem, stated as the element-wise product of two WHT transformed sequences is their logical (or dyadic) convolution [20].

Therefore, in Equation (3), it can be seen that the right-hand side is the product of two WHT transformed sequences, namely, $\boldsymbol{X}$ and diag $\{\boldsymbol{D}\}$, plus the WHT of noise vector, where diag $\{\cdot\}$ is the operation of the vector representation of the diagonal of the matrix in the argument. Therefore, after defining $\boldsymbol{d} \triangleq \text{diag}\{\boldsymbol{D}\}, \boldsymbol{X}' \triangleq \boldsymbol{W}\boldsymbol{X}$, the k^{th} entry of pre-equalization vector, $\boldsymbol{Y}$, can be written as

$$[\boldsymbol{Y}]_k = \sum_{n=0}^{N-1} [\boldsymbol{d}]_{k\oplus n}[\boldsymbol{X}']_n + \sum_{n=0}^{N-1} [\boldsymbol{W}]_{k,n}[\boldsymbol{w}]_n \tag{5}$$

The authors in [16] propose per-subchannel equalization in Hadamard domain using the equalization matrices traditionally used for conventional OFDM. In particular, let $[\boldsymbol{\Omega}_{\mathrm{ZF}}^{-1}]_{u,u} = [\boldsymbol{D}^{-1}]_{u,u}$ be the $(u,u)^{\text{th}}$ entry of diagonal ZF equalization matrix, then, after defining $\boldsymbol{B} \triangleq \boldsymbol{W}\mathrm{diag}\left\{\boldsymbol{\Omega}_{\mathrm{EQ}}^{-1}\right\}$, the equalization can be also be performed directly by dyadic convolution. In such case, the estimate of the k^{th} entry of the transmitted vector can be written as

$$[\hat{\boldsymbol{X}}]_k = \sum_{n=0}^{N-1} [\boldsymbol{B}]_{k\oplus n}[\boldsymbol{Y}]_n \; = [\boldsymbol{X}]_k + [\tilde{\boldsymbol{w}}]_k \tag{6}$$

where $[\tilde{\boldsymbol{w}}]_k$ is the noise vector and there is no intercarrier interference (ICI) term because $\boldsymbol{\Omega}_{\mathrm{EQ}}^{-1}$ is a diagonal matrix.

The dyadic convolution receiver has a relatively high computational complexity of $\mathcal{O}(N^2)$ [20] and the advantage measured in terms reduced complexity due to T-transform pair (to be discussed shortly in Subsection 2.1) is far outweighed by the complexity increase due to dyadic convolution.

Figure 1($\boldsymbol{c}$) shows a different receiver configuration where T-transform is followed by WHT transforms with single-tap equalization in between them. In this case, the the estimate of the transmitted T-OFDM vector is given as

$$\begin{aligned}\hat{\boldsymbol{X}} &= \boldsymbol{W}\boldsymbol{\Omega}_{\mathrm{EQ}}^{-1}\boldsymbol{W}\boldsymbol{W}\boldsymbol{D}\boldsymbol{W}\boldsymbol{X} + \boldsymbol{W}\boldsymbol{\Omega}_{\mathrm{EQ}}^{-1}\boldsymbol{W}\boldsymbol{W}\boldsymbol{w} \\ &= \boldsymbol{X} + \boldsymbol{W}\boldsymbol{\Omega}_{\mathrm{EQ}}^{-1}\boldsymbol{w}\end{aligned} \tag{7}$$

The receiver configuration proposed in this paper, illustrated in Figure 1 (d), decomposes the T-transform matrix into FFT and WHT transforms, with the equalization performed in between them. In particular, after the FFT transform, the received vector is given as

$$\begin{aligned}\boldsymbol{Y} &= \boldsymbol{F}\boldsymbol{H}_c\boldsymbol{T}^{\mathcal{H}}\boldsymbol{X} + \boldsymbol{F}\boldsymbol{\eta} \\ &= \boldsymbol{F}\boldsymbol{H}_c\boldsymbol{F}^{\mathcal{H}}\boldsymbol{W}\boldsymbol{X} + \boldsymbol{F}\boldsymbol{\eta} \\ &= \boldsymbol{D}\boldsymbol{W}\boldsymbol{X} + \boldsymbol{w}\end{aligned} \tag{8}$$

where in the last equality $\boldsymbol{D} = \boldsymbol{F}\boldsymbol{H}_c\boldsymbol{F}^{\mathcal{H}}$ has been used. Equalization is then performed by pre-multiplying $\boldsymbol{Y}$ with diagonal matrix $\boldsymbol{\Omega}_{\mathrm{EQ}}^{-1}$, which is followed by WHT transform to obtain the estimate of the transmitted vector, i.e.,

$$\begin{aligned}\hat{\boldsymbol{X}} &= \boldsymbol{W}\boldsymbol{\Omega}_{\mathrm{EQ}}^{-1}\boldsymbol{D}\boldsymbol{W}\boldsymbol{X} + \boldsymbol{W}\boldsymbol{\Omega}_{\mathrm{EQ}}^{-1}\boldsymbol{w} \\ &= \boldsymbol{X} + \boldsymbol{W}\boldsymbol{\Omega}_{\mathrm{EQ}}^{-1}\boldsymbol{w}\end{aligned} \tag{9}$$

Equations (6), (7) and (9) show an estimate of transmitted vector $\boldsymbol{X}$ for different receiver configurations given in Figure $1(\boldsymbol{b}), (\boldsymbol{c})$ and $(\boldsymbol{d})$, respectively. The simulation example below verifies that the three approaches of receiver-side processing of the T-OFDM have the same bit

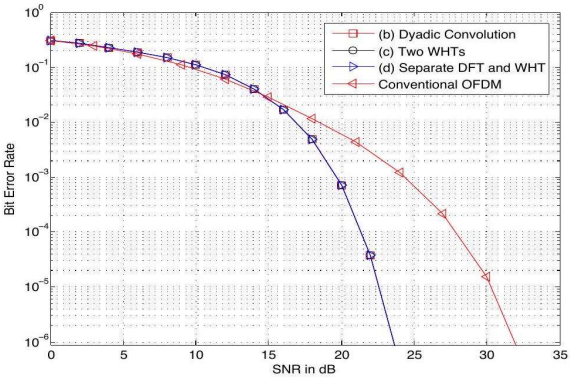

Figure 2: BER comparison of conventional OFDM with the three approaches of T-OFDM receiver shown in Figure 1, with ZF equalization, i.e., $\boldsymbol{\Omega}_{\mathrm{EQ}}^{-1} = \boldsymbol{D}^{-1}$.

error rate (BER) performance, so that they differ only in their receiver side computational complexity. Figure 2 shows the simulation result to compare the BER performance of the conventional OFDM with three different approaches of T-OFDM receiver described above. As expected, the error performance is identical for the T-OFDM systems and significantly better than the conventional OFDM.

For example, at the BER of 10^{-5}, the performance gain of T-OFDM is about 7 dB. In all simulations, the transform length of $N = 256$ is used, 16-QAM modulated symbols are transmitted across a Rayleigh fading channel which is modeled by a Stanford University Interim (SUI)-5 [21] type three-path channel with propagation delays and fading margins of $[0 \quad 4 \quad 10]\mu s$ and $[0 \quad -5 \quad -10]$ dB respectively. The channel response is assumed to remain constant for the duration of one MC symbol and the BER graphs were averaged over 1000 simulations runs.

2.1 The T-transform

A detailed discussion on the implementation of T-transform can be found in [22], where the T-transform matrix is decomposed into several sparse matrices and a butterfly
structure is proposed to implement the transform at low complexity. In particular, it shown that the total number of real additions and multiplications are respectively

$$\begin{aligned}R_{\text{Mults}} &= 2[N\log_2(N) - (2N-2)] \\ R_{\text{Adds}} &= 4[N\log_2(N) - (2N-2)],\end{aligned} \tag{10}$$

whereas, in comparison, to implement the inverse DFT and WHT separately, the total number of real multiplications and additions are respectively

$$R_{\text{Mults}} = 2[N\log_2(N)]$$
$$R_{\text{Adds}} = 5[N\log_2(N)]. \quad (11)$$

It is difficult to find the expression for $(u,v)^{\text{th}}$ entry of $\boldsymbol{T}^{\mathcal{H}}$ because the $(u,v)^{\text{th}}$ entry of $\boldsymbol{W}$ depends on binary representation of u and v. However, a few properties of its structure can be derived here. It is well known that the sum of entries of the first row as well the first column of $\boldsymbol{F}^{\mathcal{H}}$ is $\sqrt{N}$ and the sum of entries of all other rows or columns is 0. Exactly same is true for $\boldsymbol{W}$, i.e.,

$$\sum_{u=0}^{N-1}[\boldsymbol{F}^{\mathcal{H}}]_{u,v} = \sum_{v=0}^{N-1}[\boldsymbol{F}^{\mathcal{H}}]_{u,v} = \begin{cases}\sqrt{N} & u,v=0\\ 0 & u,v\neq 0\end{cases}$$
$$\sum_{u=0}^{N-1}[\boldsymbol{W}]_{u,v} = \sum_{v=0}^{N-1}[\boldsymbol{W}]_{u,v} = \begin{cases}\sqrt{N} & u,v=0\\ 0 & u,v\neq 0\end{cases} \quad (12)$$

However, when $\boldsymbol{F}^{\mathcal{H}}$ and $\boldsymbol{W}$ are multiplied, the sum of entries of all rows as well as all columns of resultant matrix is unity. In particular, the following property of the T-transform is proved here.

Lemma 1. The sum of entries of every row as well as every column of $\boldsymbol{T}^{\mathcal{H}}$ is unity, i.e.,

$$\sum_{v=0}^{N-1}[\boldsymbol{T}^{\mathcal{H}}]_{u,v} = \sum_{u=0}^{N-1}[\boldsymbol{T}^{\mathcal{H}}]_{u,v} = 1,\ \forall\, u,v \quad (13)$$

Proof. The sum of the u^{th} row of $\boldsymbol{T}^{\mathcal{H}}$ can be computed as

$$\begin{aligned}\sum_{v=0}^{N-1}[\boldsymbol{T}^{\mathcal{H}}]_{u,v} &= \sum_{v=0}^{N-1}\sum_{k=0}^{N-1}[\boldsymbol{F}^{\mathcal{H}}]_{u,k}[\boldsymbol{W}]_{k,v}\\ &= \sum_{v=0}^{N-1}[\boldsymbol{F}^{\mathcal{H}}]_{u,v}\sum_{k=0}^{N-1}[\boldsymbol{W}]_{v,k}\\ &= [\boldsymbol{F}^{\mathcal{H}}]_{u,0}\sum_{k=0}^{N-1}[\boldsymbol{W}]_{0,k}\\ &= \frac{1}{\sqrt{N}}\sqrt{N} = 1 \end{aligned} \quad (14)$$

where last equality in (14) is obtained by noting that, for any given u, the entries of $\boldsymbol{F}^{\mathcal{H}}$ repeat over k for every v, so that the entries of $\boldsymbol{F}^{\mathcal{H}}$ can be taken outside of inner summation. Then, the third equality follows because $\sum_{k=0}^{N-1}[\boldsymbol{W}]_{0,k} = \sqrt{N}$ and $\sum_{k=0}^{N-1}[\boldsymbol{W}]_{v,k} = 0$ for $v \neq 0$, so that all terms of outer summation are 0 except when $v = 0$ and $[\boldsymbol{F}^{\mathcal{H}}]_{u,0} = \frac{1}{\sqrt{N}}$ has been used in the last equality.

Using the same reasoning, the sum of u^{th} column of $\boldsymbol{T}^{\mathcal{H}}$ can be shown to be equal to unity by

$$\begin{aligned}\sum_{u=0}^{N-1}[\boldsymbol{T}^{\mathcal{H}}]_{u,v} &= \sum_{u=0}^{N-1}\sum_{k=0}^{N-1}[\boldsymbol{F}^{\mathcal{H}}]_{u,k}[\boldsymbol{W}]_{k,v}\\ &= \sum_{u=0}^{N-1}[\boldsymbol{W}]_{u,v}\sum_{k=0}^{N-1}[\boldsymbol{F}^{\mathcal{H}}]_{k,u}\\ &= [\boldsymbol{W}]_{0,v}\sum_{k=0}^{N-1}[\boldsymbol{F}^{\mathcal{H}}]_{k,0}\\ &= \frac{1}{\sqrt{N}}\sqrt{N} = 1, \end{aligned} \quad (15)$$

where $\sum_{k=0}^{N-1}[\boldsymbol{F}^{\mathcal{H}}]_{k,0} = \sqrt{N}, \sum_{k=0}^{N-1}[\boldsymbol{F}^{\mathcal{H}}]_{k,u} = 0$ for $u \neq 0$ and $[\boldsymbol{W}]_{0,v} = \frac{1}{\sqrt{N}}$ have been used. This concludes the proof of *Lemma1*. ■

3. PAPR of T-OFDM

The PAPR expression for the T-OFDM can be obtained from [18] (see *Theorem 1*) in Part I, by substituting $\boldsymbol{Q}_T = \boldsymbol{T}^{\mathcal{H}}$, so that

$$\gamma^{\text{T-OFDM}} = \frac{A_{\max}^2}{2}\max_n\left\{\left|\sum_{m=0}^{N-1} g[\boldsymbol{T}^{\mathcal{H}}]_{n,m}\right|^2\right\} \quad (16)$$

where $g \in \{\pm 1 \pm j\}$.

The PAPR expression in Equation (16) requires $[\boldsymbol{T}^{\mathcal{H}}]_{n,m}$, which is difficult to obtain because $[\boldsymbol{W}]_{u,v}$ is a function of binary representation of u and v. Therefore, computation of a closed-form expression for the PAPR of T-OFDM seems infeasible.

Numerically, the PAPR can be computed for T-OFDM for various N. In particular, Equation (16) was calculated at various N and averaged over 10^5 T-OFDM symbols and the result is summarized in the Table 1.

$$\gamma^{\text{T- OFDM}} = \frac{\max_i\left\{\max_n\{|[\boldsymbol{\Xi}_I\boldsymbol{T}^{\mathcal{H}}\boldsymbol{X}_i]_n|^2\}\right\}}{\frac{1}{N+L_P}\|\boldsymbol{\Xi}_I\boldsymbol{T}^{\mathcal{H}}\boldsymbol{X}_i\|^2}. \quad (17)$$

The table shows the PAPR of T-OFDM at various values of N expressed as a number times the $A_{\max}^2$, the PAPR of the constellation alphabet, $\mathcal{A}$. However, these results may be significantly different from the actual theoretical PAPR of T-OFDM because the likelihood that the PAPR of a particular T-OFDM symbol is equal to the theoretical maximum is very small.

Transform size, N	PAPR	PAPR (in dB) for $A_{\max}^2 = 1.8$
64	$6.19A_{\max}^2$	10.4696
128	$6.73A_{\max}^2$	10.8329
256	$7.30A_{\max}^2$	11.1860
512	$7.62A_{\max}^2$	11.3723
1024	$7.90A_{\max}^2$	11.5290

Table 1: Numerical value of the PAPR of T-OFDM at various values of N for normalized QAM constellation of size $M = 16$, so that $A_{\max}^2 = 1.8$.

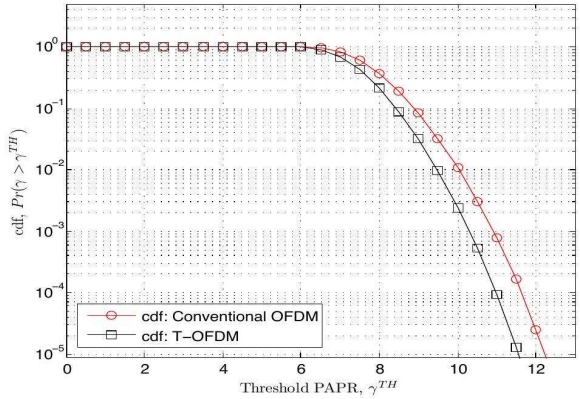

Figure 3: Graphs showing the probability that T-OFDM and the conventional OFDM will cross a given threshold level of PAPR.

To get a better insight into the PAPR of T-OFDM, Figure 3 compares the cumulative distribution functions (cdf) of the PAPRs of the conventional OFDM and T-OFDM. The two curves run approximately parallel until the threshold PAPR of $12 - 13$ dB. However, the theoretical PAPR of the conventional OFDM is $NA_{\max}^2$, so that if the two curves kept going in parallel, the PAPR of T-OFDM could also be large; it appeared relatively lower in Table 1 because of the statistical likelihood of a theoretical peak occurring is very small.

4. Error Performance

In this section, the performance of T-OFDM will be evaluated using three different performance metrics, namely, the SNR on the k^{th} subchannel, the coding gain and diversity order.

4.1 Diversity Order and Coding Gain

For an excellent work on the concepts of diversity order and coding gain for conventional OFDM, reader is directed to [23]. Here, these derivations will be carried out in detail for T-OFDM. For the sake of simplicity, the analysis is carried out here for the receiver configuration shown in Figure 1(b). However, the results do apply to the dyadic convolution receiver configuration as well because of the equivalence of the two systems.

Let $\boldsymbol{Y} \triangleq \boldsymbol{F}\boldsymbol{H}_c\boldsymbol{T}^{\mathcal{H}}\boldsymbol{X}$ denote the received vector when the symbol $\boldsymbol{X}$ is correctly recovered and $\tilde{\boldsymbol{Y}} \triangleq \boldsymbol{F}\boldsymbol{H}_c\boldsymbol{T}^{\mathcal{H}}\tilde{\boldsymbol{X}}$ denote the case when the $\boldsymbol{X}$ is incorrectly received as $\tilde{\boldsymbol{X}}$, with $\boldsymbol{e} \triangleq \boldsymbol{X} - \tilde{\boldsymbol{X}} \neq \boldsymbol{0}_{N\times 1}$ being the error vector. Then, the upper bound on the pairwise error probability (PEP) is given as [5]

$$P\left(\boldsymbol{X} \to \tilde{\boldsymbol{X}} \mid \boldsymbol{h}\right) \leq \exp\left(\frac{-d^2\left(\boldsymbol{Y}, \tilde{\boldsymbol{Y}}\right)}{4N_o}\right) \tag{18}$$

where $d(\boldsymbol{Y}, \tilde{\boldsymbol{Y}}) = \| \boldsymbol{Y} - \tilde{\boldsymbol{Y}} \|$ is the Euclidean distance between the two vectors, which is,

$$\begin{aligned} \| \boldsymbol{Y} - \tilde{\boldsymbol{Y}} \| &= \|\boldsymbol{F}\boldsymbol{H}_c\boldsymbol{T}^{\mathcal{H}}\boldsymbol{X} - \boldsymbol{F}\boldsymbol{H}_c\boldsymbol{T}^{\mathcal{H}}\tilde{\boldsymbol{X}}\| \\ &= \|\boldsymbol{F}\boldsymbol{H}_c\boldsymbol{F}^{\mathcal{H}}\boldsymbol{W}\boldsymbol{X} - \boldsymbol{F}\boldsymbol{H}_c\boldsymbol{F}^{\mathcal{H}}\boldsymbol{W}\tilde{\boldsymbol{X}}\| \\ &= \| \boldsymbol{D}\boldsymbol{W}(\boldsymbol{X} - \tilde{\boldsymbol{X}}) \| \\ &= \|\text{Diag}\,\{\boldsymbol{V}_L\boldsymbol{h}\}\boldsymbol{D}_e\|, \\ &= \|\boldsymbol{D}_X\boldsymbol{V}_L\boldsymbol{h}\| \end{aligned} \tag{19}$$

where, in fourth equality in Equation (18), $\boldsymbol{V}_L$ is an $N \times L$ sized matrix with $[\boldsymbol{V}_L]_{u,v} = e^{-j\frac{2\pi}{N}uv}$, i.e., the last $N - L$ columns of $\sqrt{N}\boldsymbol{F}$ are truncated, so that $\boldsymbol{D} \triangleq \text{Diag}\,\{\boldsymbol{V}_L\boldsymbol{h}\}$ and $\boldsymbol{D}_e \triangleq \boldsymbol{W}(\boldsymbol{X} - \tilde{\boldsymbol{X}}) = \boldsymbol{W}\boldsymbol{e}$. The last equality in (18) follows after forming diagonal matrix from $\boldsymbol{D}_e$ by $\boldsymbol{D}_X \triangleq \text{Diag}\,\{\boldsymbol{D}_e\}$ and bringing it in the front and writing the diagonal of Diag $\{\boldsymbol{V}_L\boldsymbol{h}\}$ as vector at the end.

The square of the Euclidean distance can then be written as

$$\begin{aligned} d^2(\boldsymbol{Y} - \tilde{\boldsymbol{Y}}) &= \|\boldsymbol{D}_X\boldsymbol{V}_L\boldsymbol{h}\|^2 = (\boldsymbol{D}_X\boldsymbol{V}_L\boldsymbol{h})^{\mathcal{H}}(\boldsymbol{D}_X\boldsymbol{V}_L\boldsymbol{h}) \\ &= \boldsymbol{h}^{\mathcal{H}}\boldsymbol{V}_L^{\mathcal{H}}\boldsymbol{D}_X^{\mathcal{H}}\boldsymbol{D}_X\boldsymbol{V}_L\boldsymbol{h} \\ &= \boldsymbol{h}^{\mathcal{H}}\boldsymbol{A}_e\boldsymbol{h}, \end{aligned} \tag{20}$$

where $\boldsymbol{A}_e \triangleq \boldsymbol{V}_L^{\mathcal{H}}\boldsymbol{D}_X^{\mathcal{H}}\boldsymbol{D}_X\boldsymbol{V}_L$. Then an upper bound on the PEP is given as [5]

$$P\left(\boldsymbol{X} \to \tilde{\boldsymbol{X}} \mid \boldsymbol{h}\right) \leq \left(\frac{1}{4N_o}\right)^{r_e-1}\left(\prod_{l=0}^{r_e-1}\lambda_{e,l}\right)^{-1} \tag{21}$$

where r_e is the rank of matrix $\boldsymbol{A}_e$ and $\lambda_{e,l} > 0$ are the non-decreasing eigenvalues of $\boldsymbol{A}_e$.

Using the reasoning in [5], the diversity order and coding gain of T-OFDM can be obtained as functions of matrix $\boldsymbol{A}_e$ and are given respectively by

$$\begin{aligned} G_d &\triangleq \min_{\boldsymbol{e}\neq\boldsymbol{0}} \ \text{rank}\,(\boldsymbol{A}_e) \\ G_c &\triangleq \min_{\boldsymbol{e}\neq\boldsymbol{0}} \left(\prod_{l=0}^{r_e-1} \lambda_{e,l}\right)^{1/r_e} \\ &= \min_{\boldsymbol{e}\neq\boldsymbol{0}} \det(\boldsymbol{A}_e)^{\frac{1}{r_e}} \end{aligned} \tag{22}$$

where the last equality in Equation (22) follows because the product of eigenvalues of a matrix is equal to its determinant.

4.1.1 T-OFDM Diversity Order

Equations (21) and (22) suggest that the error performance of T-OFDM will improve as the rank and determinant of $\boldsymbol{A}_e$ increase. It is possible to further evaluate these expressions and show that T-OFDM has the *maximum possible coding gain and diversity order*. In particular, since the order of matrix $\boldsymbol{V}_L$ is $N \times L$, the order of $\boldsymbol{A}_e$ is $L \times L$, so that the maximum diversity order achievable is also L.

Furthermore, since the matrix $\boldsymbol{A}_e = (\boldsymbol{D}_X\boldsymbol{V}_L)^{\mathcal{H}}\boldsymbol{D}_X\boldsymbol{V}_L$ is a Gram matrix (the Gram matrix of $\boldsymbol{X}$ is given by $\boldsymbol{X}\boldsymbol{X}^{\mathcal{H}}$, with $\text{rank}\,(\boldsymbol{X}) = \text{rank}\,(\boldsymbol{X}\boldsymbol{X}^{\mathcal{H}})$, see, for example, 46]), it can be said that

$$\begin{aligned} r_e &= \text{rank}\,(\boldsymbol{A}_e) = \text{rank}\,((\boldsymbol{D}_X\boldsymbol{V}_L)^{\mathcal{H}}\boldsymbol{D}_X\boldsymbol{V}_L) \\ &= \text{rank}\,(\boldsymbol{D}_X\boldsymbol{V}_L) \\ &= \text{rank}(\text{Diag}\{\boldsymbol{W}\boldsymbol{e}\}\boldsymbol{V}_L). \end{aligned} \tag{23}$$

Now, for two complex matrices $\boldsymbol{A}$ and $\boldsymbol{B}$, if matrix $\boldsymbol{A}$ is a full rank and $\boldsymbol{B}$ is conformable for the product $\boldsymbol{A}\boldsymbol{B}$, then $\text{rank}\,(\boldsymbol{A}\boldsymbol{B}) = \text{rank}\,(\boldsymbol{B})$ (see [24]). Matrix $\boldsymbol{V}_L$ is by definition full rank, i.e., $\text{rank}\,(\boldsymbol{V}_L) = L$. Thus, to show that $\boldsymbol{A}_e$ is full rank, it should be shown that $\text{rank}\,(\text{Diag}\,\{\boldsymbol{W}\boldsymbol{e}\}) \geq L$, which in turn requires it to be shown that it has at least L non-zero entries on its diagonal because it is a diagonal matrix.

Consider first the case when $\boldsymbol{e}$ has only one non-zero entry at the k^{th} position and denote it with $\boldsymbol{e}_k, \boldsymbol{e}_k \triangleq [\boldsymbol{0}_{1,k-1} \quad g \quad \boldsymbol{0}_{1,N-k-1}]^{\mathcal{T}}, g \in \mathbb{C}, g \neq 0$, then it can be seen that $[\text{Diag}\,\{\boldsymbol{W}\boldsymbol{e}_k\}]_{n,n} = g[\boldsymbol{W}]_{n,k} \neq 0, \forall n$, by the definition of g and $\boldsymbol{W}$, so that $\text{rank}\,(\text{Diag}\,\{\boldsymbol{W}\boldsymbol{e}_k\}) = N$.

To generalize it for any $\boldsymbol{e}$ with $1 \leq K \leq N$ non-zero entries, it can be seen that

$$[\text{Diag}\,\{\boldsymbol{W}\boldsymbol{e}_k\}]_{u,u} = [\boldsymbol{W}]_{u,}, \boldsymbol{e} \tag{24}$$

i.e., the inner product of u^{th} row of $\boldsymbol{W}$ and $\boldsymbol{e}$. For a given combination of entries in $\boldsymbol{e}$, this product cannot be 0 for more than one rows because the rows of $\boldsymbol{W}$ are orthogonal. Therefore, $\text{rank}\,(\text{Diag}\,\{\boldsymbol{W}\boldsymbol{e}_k\}) \geq L$ for every $\boldsymbol{e}$. Thus, $r_e = L$ for the T-OFDM and hence it achieves maximum diversity order.

4.1.2 T-OFDM Coding Gain

To find the coding gain for T-OFDM and show that it indeed achieves maximum coding gain, upper and lower bounds on coding gain should first be derived. Recall the expression for coding gain

$$G_c = \min_{\boldsymbol{e}\neq\boldsymbol{0}} \det(\boldsymbol{A}_e)^{\frac{1}{r_e}} \tag{25}$$

By the definition of matrix $\boldsymbol{A}_e$, it is a Toeplitz matrix with all diagonal entries equal to $\| \boldsymbol{W}\boldsymbol{e} \|^2$ [23]. The Hadamard inequality, which states the determinant of a matrix is less than or equal to the product of diagonal entries of the matrix [25], can be used here to get

$$\begin{aligned} \det\,(\boldsymbol{A}_e) &\leq \| \boldsymbol{W}\boldsymbol{e} \|^{2L} \\ \Rightarrow G_c &\leq \min_{\boldsymbol{e}\neq\boldsymbol{0}} \| \boldsymbol{W}\boldsymbol{e} \|^{\frac{2L}{r_e}} \end{aligned} \tag{26}$$

The minimum value of $\| \boldsymbol{W}\boldsymbol{e} \|^{2L}$ will be obtained during the single-error event. In particular, define $d^2_{\mathcal{A}_{\min}} = \min\{|a_1 - a_2|^2 \mid a_1, a_2 \in \mathcal{A}, a_1 \neq a_2\}$, the minimum Euclidean distance between any two constellation points and assume only one non-zero entry in $\boldsymbol{e}$ at the k^{th} position, i.e., $\boldsymbol{e}_k = [\boldsymbol{0}_{1,k-1} \quad d_{\mathcal{A}_{\min}} \quad \boldsymbol{0}_{1,N-k-1}]^{\mathcal{T}}$. In this case,

$$\| \boldsymbol{W}\boldsymbol{e} \|^{2L} = \left\| d_{\mathcal{A}_{\min}} [\boldsymbol{W}]_{,k} \right\|^{2L} = d^{2L}_{\mathcal{A}_{\min}} \tag{27}$$

because the norm of the k^{th} column of $\boldsymbol{W}$ is unity. Thus, the coding gain of T-OFDM is upper bounded by

$$G_c \leq d^{\frac{2L}{r_e}}_{\mathcal{A}_{\min}}. \tag{28}$$

4.2 SNR per Subchannel

The SNR on the k^{th} subchannel was derived in [16]. However, it was not demonstrated that T-OFDM is optimal in terms of error performance. To find the SNR on the k^{th} subchannel of T-OFDM, recall from Equation (31) in [18]

of this series, the expression for the SNR on the k^{th} subchannel of ZF equalized GMC system

$$\beta_k^{\text{ZF,GMC}} = \beta_o \cdot \frac{\prod_{m=0}^{N-1} \left|[\boldsymbol{D}]_{m,m}\right|^2}{\sum_{n=0}^{N-1} \left(\left|[\boldsymbol{Q}_R \boldsymbol{F}^{\mathcal{H}}]_{k,n}\right|^2 \prod_{m=0,m\neq n}^{N-1} \left|[\boldsymbol{D}]_{m,m}\right|^2\right)} \quad (29)$$

and substitute $\boldsymbol{Q}_R = \boldsymbol{T} = \boldsymbol{WF}$ to obtain

$$\begin{aligned}\beta_k^{\text{ZF,T-OFDM}} &= \beta_o \frac{\prod_{m=0}^{N-1} \left|[\boldsymbol{D}]_{m,m}\right|^2}{\sum_{n=0}^{N-1} \left(\left|[\boldsymbol{WFF}^H]_{\boldsymbol{k,n}}\right|^2 \prod_{\boldsymbol{m=0,m\neq n}}^{\boldsymbol{N-1}} \left|[\boldsymbol{D}]_{\boldsymbol{m,m}}\right|^2\right)} \\ &= \beta_o \frac{\prod_{m=0}^{N-1} \left|[\boldsymbol{D}]_{m,m}\right|^2}{\sum_{n=0}^{N-1} \left(\left|[\boldsymbol{W}]_{k,n}\right|^2 \prod_{m=0,m\neq n}^{N-1} \left|[\boldsymbol{D}]_{m,m}\right|^2\right)} \\ &= \beta_o \frac{N \prod_{m=0}^{N-1} \left|[\boldsymbol{D}]_{m,m}\right|^2}{\sum_{n=0}^{N-1} \prod_{m=0,m\neq n}^{N-1} \left|[\boldsymbol{D}]_{m,m}\right|^2} \\ &= \beta_o \frac{N}{\sum_{n=0}^{N-1} \left|[\boldsymbol{D}]_{n,n}\right|^2} \\ &= \beta_k^{\text{ZF,SC-FDE}} \end{aligned} \quad (30)$$

where in third equality of (28), $\left|[\boldsymbol{W}]_{k,n}\right|^2 = \frac{1}{N}, \forall k,n$, has been used and fourth equality follows by dividing both numerator and denominator with $\prod_{m=0}^{N-1}\left|[\boldsymbol{D}]_{m,m}\right|^2$.

It can be seen from Equation (30) that, like SC-FDE, the SNR on all the subchannels of T-OFDM is identical. Furthermore, the SNR of T-OFDM on the k^{th} subchannel is identical to that of SC-FDE. Since the SC-FDE has optimal performance in terms of SNR per subchannel [26], it follows that the T-OFDM system also has optimal performance with respect to ZF equalization.

To get the SINR on the k^{th} subchannel of T-OFDM using MMSE equalizer, recall the expression SINR on the k^{th} subchannel of GMC system from Equation (53) from Part I in this series

$$\tilde{\beta}_k^{\text{MMSE,GMC}} = \frac{\left|[\boldsymbol{Q}_R \boldsymbol{F}^H \boldsymbol{PDFQ}_T]_{k,k}\right|^2}{\sum_{n=0,n\neq k}^{N-1} \left|[\boldsymbol{Q}_R \boldsymbol{F}^H \boldsymbol{PDFQ}_T]_{k,n}\right|^2 + N_o \sum_{n=0}^{N-1} \left|[\boldsymbol{Q}_R \boldsymbol{F}^{\mathcal{H}} \boldsymbol{P}]_{k,n}\right|^2}. \quad (31)$$

and again replacing $\boldsymbol{Q}_T = \boldsymbol{T}^{\mathcal{H}} = \boldsymbol{F}^{\mathcal{H}}\boldsymbol{W}^{\mathcal{H}}$ and $\boldsymbol{Q}_R = \boldsymbol{T} = \boldsymbol{WF}$ to get the Equation (32) at the top of next page.

It is difficult to obtain further closed form simplifications of this SNR expression in Equation (32). At high value of β_o, however, this expression can be simplified. To compare the MMSE and ZF SNR on the k^{th} subchannel of T-OFDM at large value of β_o, such a simplification is carried out here.

In particular, since both $\boldsymbol{P}$ and $\boldsymbol{D}$ are diagonal, their product is also diagonal. Recalling from Equation (42) from [18] that $[\boldsymbol{P}]_{u,u} = \frac{\beta_o[\boldsymbol{D}^{\mathcal{H}}]_{u,u}}{\beta_o[\boldsymbol{DD}^{\mathcal{H}}]_{u,u}+1}$, it can be seen that $[\boldsymbol{PD}]_{u,u} = \frac{\beta_o[\boldsymbol{DD}^{\mathcal{H}}]_{u,u}}{\beta_o[\boldsymbol{DD}^{\mathcal{H}}]_{u,u}+1} = \frac{\beta_o|[\boldsymbol{D}]_{u,u}|^2}{\beta_o|[\boldsymbol{D}]_{u,u}|^2+1}$. At high SNR such that $\beta_o\left|[\boldsymbol{D}]_{u,u}\right|^2 >> 1, \forall u$, it can be seen that $[\boldsymbol{PD}]_{u,u} \approx 1$ and $\boldsymbol{PD} \approx \boldsymbol{I}_N \Rightarrow \boldsymbol{WPDW}^{\mathcal{H}} \approx \boldsymbol{I}_N$. In such case, the numerator of Equation (32) can be approximated as 1 for all k and first summation in the denominator can be approximated as 0, for all k, because summation does not allow $n = k$. Thus, the SNR on the k^{th} subchannel can be approximated as

$$\begin{aligned}\beta_k^{\text{MMSE, T-OFDM}} &\approx \frac{1}{N_o \sum_{n=0}^{N-1} \left|[\boldsymbol{WP}]_{k,n}\right|^2} \\ &= \beta_o \frac{1}{\sum_{n=0}^{N-1} \left|[\boldsymbol{W}]_{k,n}[\boldsymbol{P}]_{n,n}\right|^2} \\ &= \beta_o \frac{1}{\sum_{n=0}^{N-1} \left|[\boldsymbol{W}]_{k,n}\right|^2 \left|[\boldsymbol{P}]_{n,n}\right|^2} \\ &= \beta_o \frac{N}{\sum_{n=0}^{N-1} \left|\frac{\beta_o[\boldsymbol{D}^{\mathcal{H}}]_{n,n}}{\beta_o[\boldsymbol{D}]_{n,n}[\boldsymbol{D}^{\mathcal{H}}]_{n,n}+1}\right|^2}, \end{aligned} \quad (33)$$

where second equality in (33) follows because the $\boldsymbol{P}$ is diagonal. Using $\beta_o\left|[\boldsymbol{D}]_{u,u}\right|^2 >> 1 \Rightarrow \beta_o[\boldsymbol{D}]_{n,n}[\boldsymbol{D}^{\mathcal{H}}]_{n,n} + 1 \approx \beta_o[\boldsymbol{D}]_{n,n}[\boldsymbol{D}^{\mathcal{H}}]_{n,n}$, the approximate SNR on the k^{th} subchannel can be written as,

$$\begin{aligned}\beta_k^{\text{MMSE,T-OFD}} &\approx \beta_o \cdot \frac{N}{\sum_{n=0}^{N-1} \frac{1}{\left|[\boldsymbol{D}]_{n,n}\right|^2}} \\ &= \beta_o \cdot \frac{N \prod_{m=0}^{N-1} \left|[\boldsymbol{D}]_{m,m}\right|^2}{\sum_{n=0}^{N-1} \prod_{m=0,m\neq n}^{N-1} \left|[\boldsymbol{D}]_{m,m}\right|^2} \\ &= \beta_k^{\text{ZF,T- OFDM}}. \end{aligned} \quad (34)$$

Thus, it can be seen that at high SNR, the MMSE and ZF equalizers have identical performance for the T-OFDM system, which is generally expected for the two equalization schemes.

5. Timing Synchronization Errors

In *Theorem 2* of [18], the conditions over $\boldsymbol{Q}_T \mid \boldsymbol{Q}_R$ based GMC system were presented that allowed identical performance to that of conventional OFDM due to timing error, ζ, when it holds following bound: $L_P - L \leq \zeta \leq 0$. The two conditions proved in the theorem were:

a) $\boldsymbol{Q}_R$ is N-periodic and $[\boldsymbol{Q}]_{u,v+\zeta} = g\left(K_u, [\boldsymbol{Q}]_{u,v}\right)$, where K_u is independent of v but same for all entries of u^{th}

row, and $g(\cdot,\cdot)$ is an arithmetic operation between the arguments, or

b) $\boldsymbol{Q}_R$ itself does not satisfy condition (a) but it can be expressed as $\boldsymbol{Q}_R = \tilde{\boldsymbol{Q}}_R \boldsymbol{\Psi}$, where $\tilde{\boldsymbol{Q}}_R$ satisfies condition $(\boldsymbol{a})$ and $\boldsymbol{\Psi}$ is N-periodic.

To see the applicability of this theorem to $\boldsymbol{T} = \boldsymbol{WF}$, first it should be checked if $\boldsymbol{T}$ is periodic. It was shown in the *Lemma 3* in [18] of this three-paper series, that product of two N-periodic matrices is also N-periodic.

$$\tilde{\beta}_k^{\text{MMSE, T-OFDM}} = \frac{\left|[\boldsymbol{WFF}^{\mathcal{H}}\boldsymbol{PDFF}^{\mathcal{H}}\boldsymbol{W}^{\mathcal{H}}]_{k,k}\right|^2}{\sum_{n=0,n\neq k}^{N-1}\left|[\boldsymbol{WFF}^{\mathcal{H}}\boldsymbol{PDFF}^{\mathcal{H}}\boldsymbol{W}^{\mathcal{H}}]_{k,n}\right|^2 + N_o\sum_{n=0}^{N-1}\left|[\boldsymbol{WFF}^{\mathcal{H}}\boldsymbol{P}]_{k,n}\right|^2} = \frac{\left|[\boldsymbol{WPDW}^{\mathcal{H}}]_{k,k}\right|^2}{\sum_{n=0,n\neq k}^{N-1}\left|[\boldsymbol{WPDW}^{\mathcal{H}}]_{k,n}\right|^2 + N_o\sum_{n=0}^{N-1}\left|[\boldsymbol{WP}]_{k,n}\right|^2}. \quad (32)$$

The matrix $\boldsymbol{F}$ is already well-known to be N-periodic. To check the periodicity of $\boldsymbol{W}$, for $c = \log_2 N$, recall the $(u,v)^{\text{th}}$ entry of $\boldsymbol{W}$ is given as

$$[\boldsymbol{W}]_{u,v} = \frac{1}{\sqrt{N}}\prod_{i=0}^{c-1}(-1)^{u_i v_i} \quad (35)$$

where u_i and v_i represent the i^{th} bits of the binary representation of u and v. To see, it periodicity,

$$\begin{aligned}[\boldsymbol{W}]_{u+pN,v+q} &= \frac{1}{\sqrt{N}}\prod_{i=0}^{c-1}(-1)^{(u+pN)_i(v+qN)_i} \\ &= \frac{1}{\sqrt{N}}\prod_{i=0}^{c-1}(-1)^{u_i v_i} \\ &= [\boldsymbol{W}]_{u,v}, \end{aligned} \quad (36)$$

where the second equality follows because the first c bits of binary representation of both pN and qN are all 0s for any integers p and q as N is necessarily a power of 2. This shows the WHT matrix is N-periodic and therefore the matrix $\boldsymbol{T}$ is also N-periodic [18].

However, the matrix $\boldsymbol{T}$ still does not satisfy either of the conditions required on $\boldsymbol{Q}_R$ specified above. It is easy to see that, the matrix $\boldsymbol{W}$, whose $(u,v)^{\text{th}}$ entry depends on the binary representation of u and v, does not satisfy the condition $(\boldsymbol{a})$. Therefore, $\boldsymbol{T} = \boldsymbol{WF}$ also does not satisfy the condition $(\boldsymbol{a})$. To check for the condition $(\boldsymbol{b})$, since the product of $\boldsymbol{W}$ and $\boldsymbol{F}$ is not commutative, i.e., $\boldsymbol{WF} \neq \boldsymbol{FW}$, it can be seen that $\tilde{\boldsymbol{Q}}_R = \boldsymbol{F}$ and $\boldsymbol{\Psi} = \boldsymbol{W}$. While $\boldsymbol{Q}_R = \boldsymbol{F}$ is periodic, $\boldsymbol{\Psi} = \boldsymbol{W}$ does not satisfy the condition (a). Thus, the matrix $\boldsymbol{T}$ does not satisfy either of the conditions. Thus, even for a small timing error, the T-OFDM system will incur ISI in the receiver configuration suggested in its original work [22], where the T-transform is implemented at the receiver. Following simulation example verifies above discussion.

Figure 4 compares the conventional OFDM and T-OFDM for sensitivity to timing synchronization errors. For timing error of only one sample, $|\zeta| = 1$, the figure plots the received complex alphabet symbols after the FFT and T-transforms for conventional and T-OFDM, respectively. As can be seen, conventional OFDM incurs only a phase rotation (square 16-QAM constellation at transmitter turns into a constellation with three concentric circles), which can be corrected along with single-tap equalization. For the case of T-OFDM, constellation points cannot be reconstructed easily.

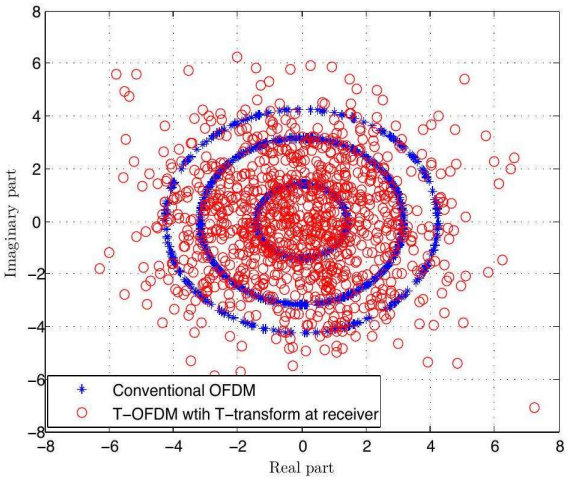

Figure 4: Received complex symbols after DFT and T-transforms plotted on constellation when $N = 1024$ and $|\zeta| = 1$.

To avoid this performance degradation due to timing errors in T-OFDM, the proposed receiver configuration can be used (see Figure 1(d)). In particular, after the FFT, the phase rotation (as shown in Figure 4) can be corrected along with single-tap equalization, which can then be followed by the WHT transform. Thus, besides reducing the complexity of the receiver, the proposed receiver configuration alleviates the sensitivity of T-OFDM system against the timing errors.

6. Conclusions

This paper studied the T-OFDM system with various receiver configuration. The PAPR performance of the T-OFDM was also studied using both analytical expressions and simulation results. It was shown using the SNR per subchannel that T-OFDM is optimal in error performance. The diversity order and coding gain of T-OFDM were also investigated, resulting in new closed form expressions. Simulation results showed that the error performance of T-OFDM matches that of SC-FDE system. An upper bound on the SNR in the presence of CFO was also derived.

References

[1] 3GPP. "5G; NR; Physical Channels and Modulation." 3rd Generation Partnership Project (3GPP), TS 38.211, v15.2.0, June 2018.

[2] IEEE. "IEEE Standard for Information Technology—Telecommunications and Information Exchange Between Systems—Local and Metropolitan Area Networks—Specific Requirements—Part 11: Wireless LAN Medium Access Control (MAC) and Physical Layer (PHY) Specifications." IEEE Std 802.11-2016 (Revision of IEEE Std 802.11-2012), 1-3534, Dec. 2016.

[3] Sun, Y. "Bandwidth-Efficient Wireless OFDM." IEEE Journal on Selected Areas in Communications 19, no. 11 (2001): 2267–2278.

[4] Peled, A., and A. Ruiz. "Frequency Domain Data Transmission Using Reduced Computational Complexity Algorithms." In Proceedings of IEEE International Conference on Acoustics, Speech, and Signal Processing (ICASSP), 964–967. Denver, CO, USA, April 1980.

[5] Wang, Z., and G. B. Giannakis. "Complex-Field Coding for OFDM over Fading Wireless Channels." IEEE Transactions on Information Theory 49, no. 3 (2003): 707–720.

[6] Bäuml, R. W., R. F. H. Fischer, and J. B. Huber. "Reducing the Peak-to-Average Power Ratio of Multicarrier Modulation by Selected Mapping." Electronics Letters 32, no. 22 (1996): 2056–2057.

[7] Moose, P. H. "A Technique for Orthogonal Frequency Division Multiplexing Frequency Offset Correction." IEEE Transactions on Communications 42, no. 10 (1994): 2908–2914.

[8] Muller, S. H., R. W. Bäuml, R. F. H. Fischer, and J. B. Huber. "OFDM with Reduced Peak-to-Average Power Ratio by Multiple Signal Representation." Annales des Télécommunications 52, no. 1-2 (1997): 58–67.

[9] Shao, X., R. Schiphorst, and C. H. Slump. "An Opportunistic Error Correction Layer for OFDM Systems." EURASIP Journal on Wireless Communications and Networking 2009, pp. 1–10, Jan. 2009.

[10] Chang, M. X., and T. D. Hsieh. "Detection of OFDM Signals in Fast-Varying Channels with Low-Density Pilot Symbols." IEEE Transactions on Vehicular Technology 57, no. 2 (2008): 859–872.

[11] Mandyam, G. "Sinusoidal Transforms in OFDM Systems." IEEE Transactions on Broadcasting 50, no. 2 (2004): 172–184.

[12] Wang, D., D. Liu, F. Liu, and G. Yue. "A Novel DHT-Based Ultra-Wideband System." In Proceedings of IEEE International Symposium on Communications and Information Technology, 672–675. Beijing, China, October 2005.

[13] Jao, C., S. Long, and M. Shiue. "DHT-Based OFDM System for Passband Transmission over Frequency-Selective Channel." IEEE Signal Processing Letters 17, no. 8 (2010): 699–702.

[14] Ahmed, M. S., S. Boussakta, B. Sharif, and C. C. Tsimenidis. "OFDM Based on Low Complexity Transform to Increase Multipath Resilience and Reduce PAPR." IEEE Transactions on Signal Processing 59, no. 12 (2011): 5994–6007.

[15] Ali, I., A. Pollok, L. Luo, and L. Davis. "A Low Complexity Receiver for T-Transform Based OFDM Systems." In Proceedings of IEEE 22nd International Symposium on Personal Indoor and Mobile Radio Communications, 1611–1615. Toronto, Canada, 2011.

[16] Ahmed, M., S. Boussakta, B. Sharif, and C. Tsimenidis. "OFDM Based New Transform with BER Performance Improvement Across Multipath Transmission." In Proceedings of IEEE International Conference on Communications, 1–5. Cape Town, South Africa, May 2010.

[17] Baig, I., and V. Jeoti. "PAPR Analysis of DHT-Precoded OFDM System for M-QAM." In Proceedings of International Conference on Intelligent and Advanced Systems (ICIAS), 1–4. Kuala Lumpur, Malaysia, 2010.

[18] Ali, I. "A Generalized Multicarrier Communication System—Part I: Theoretical Performance Analysis and Bounds," International Journal of Computer Science and Network Security 24, no. 9 (2024): 1–11.

[19] Nee, R. V., and A. de Wild. "Reducing the Peak-to-Average Power Ratio of OFDM." In Proceedings of 48th IEEE Vehicular Technology Conference, 2072–2076. Ottawa, Canada, 1998.

[20] Robinson, G. "Logical Convolution and Discrete Walsh and Fourier Power Spectra." IEEE Transactions on Audio and Electroacoustics 20, no. 4 (1972): 271–280.

[21] Erceg, V., K. Hari, M. Smith, C. Tappenden, J. Costa, D. Baum, and C. Bushue. "Channel Models for Fixed Wireless Applications." In IEEE 802.16 Broadband Wireless Access Working Group, 2001.

[22] Ahmed, M. S., S. Boussakta, B. Sharif, and C. C. Tsimenidis. "OFDM Based on Low Complexity Transform to Increase Multipath Resilience and Reduce PAPR." IEEE Transactions on Signal Processing 59, no. 12 (2011): 5994–6007.

[23] Wang, Z., X. Ma, and G. B. Giannakis. "OFDM or Single-Carrier Block Transmissions?" IEEE Transactions on Communications 52, no. 3 (2004): 380–394.

[24] Gentle, J. E. Matrix Algebra. Springer Publishing, 2007.

[25] Garling, D. J. H. Inequalities. Cambridge University Press, July 2007.

[26] Lin, Y., and S. Phoong. "BER Minimized OFDM Systems with Channel Independent Precoders." IEEE Transactions on Signal Processing 51, no. 9 (2003): 2369–2380.

Dr. Imran Ali received the B.E. in Telecommunications from Mehran University of Engineering and Technology, Pakistan, an M.Sc. degree in Electronics and Communication Engineering from Myongji University, South Korea and PhD in Telecommunications from University of South Australia. Much of his academic research has been focused on signal processing for wireless communications. He is currently an independent researcher based in Melbourne, Australia.